Available online at www.sciencedirect.com

ScienceDirect

Current Opinion in Chemical Biology

Chemiluminescent spiroadamantane-1,2-dioxetanes: Recent advances in molecular imaging and biomarker detection

Husain N. Kagalwala, R. Tate Reeves and Alexander R. Lippert

Abstract

Triggered chemiluminescence emission of spiroadamantane-1,2-dioxetanes to detect bioanalytes has fueled the emerging popularity of chemiluminescence imaging in live animals and cells. Recently, a structural evolution of the dioxetane scaffolds towards near-infrared emitters has been observed, and efforts have been made for quantitative and semi-quantitative detection of a wide range of analytes. In this review, we summarize the current chemiluminescence imaging developments of spiroadamantane-1,2-dioxetanes. Specifically, we look at examples which depict whole animal or cellular chemiluminescence imaging of small molecules and enzymes, as well as those that portray their potential diagnostic and therapeutic abilities, with an emphasis on analyte quantification and experimental parameters.

Addresses

Department of Chemistry, Southern Methodist University, Dallas, TX 75275-0314, United States

Corresponding author: Lippert, Alexander R (alippert@smu.edu)

Current Opinion in Chemical Biology 2022, **68**:102134

This review comes from a themed issue on **Molecular Imaging**

Edited by **Pablo Rivera-Fuentes** and **Claire Deo**

For a complete overview see the Issue and the Editorial

Available online xxx

https://doi.org/10.1016/j.cbpa.2022.102134

Keywords

Chemiluminescence, Spiroadamantane-1,2-dioxetanes, *In vivo* imaging, Chemiluminescence microscopy.

Abbreviations

CIEEL, chemically initiated electron exchange luminescence; NIR, near-infrared; IV, intravenous; IP, intraperitoneal; IT, intratumoral; HK-2, human kidney-2; NK, natural killer; AIE, aggregation-induced emission; FAP-α, fibroblast activation protein α; ALP, alkaline phosphatase; AMPPD, 3-[(2-spiroadamatane)-4-methoxy-4-(3-phosphoryloxy)-phenyl]-1,2-dioxetane; Mtb, *mycobacterium tuberculosis*; PSA, prostate specific antigen; DUB, deubitiquitinating enzyme; FLASH, fast, luminescent and affordable sensor of Hip-1.

Introduction

The last decade has seen the emergence of chemiluminescence (light generation from an excited state formed in a chemical reaction) as an innovative tool for imaging and sensing of biological analytes in unprocessed specimens and samples [1,2]. Unlike their fluorescent counterparts [3,4], chemiluminescent probes are less prone to autofluorescence or light scattering, providing better signal-to-noise ratios and imaging depth. Of the different classes of chemiluminescent molecules [5], phenolate spiroadamantane-1,2-dioxetanes [6–8] have gained special attention, mainly due to the thermal stability of the sterically restricted molecules and their reaction-based ability to detect biologically relevant signaling ions and molecules [9]. The trigger generally involves removal of a protecting group or substrate, which is attached to the phenol either directly or through a self-immolative linker. This, in turn, results in chemiluminescence via the proposed chemically initiated electron exchange luminescence (CIEEL) mechanism (Figure 1a) [10,11], although the possibility of other mechanistic pathways have not been ruled out [12].

Of late, a push towards the development of near-infrared emitting probes has been made given the better penetration depth at longer wavelengths (Figure 1b). Successful strategies include encapsulation [13,14], direct modification of the dioxetane scaffold [15], or conjugation of red-emitting dyes [16], the latter resulting in a ratiometric response via energy transfer. In addition, bioanalyte quantification and probe kinetics are also being increasingly investigated [17]. This review highlights the recent advances of chemiluminescent spiroadamantane-1,2-dioxetanes in bioimaging. Specifically, we highlight literature examples from recent years that involve chemiluminescence microscopy and/or *in vivo* imaging of small molecules and enzymes. We also look at other applications such as microbe detection which do not require imaging but are likely to have a deep impact. Finally, we summarize factors like the type of injection, time course of the

Figure 1

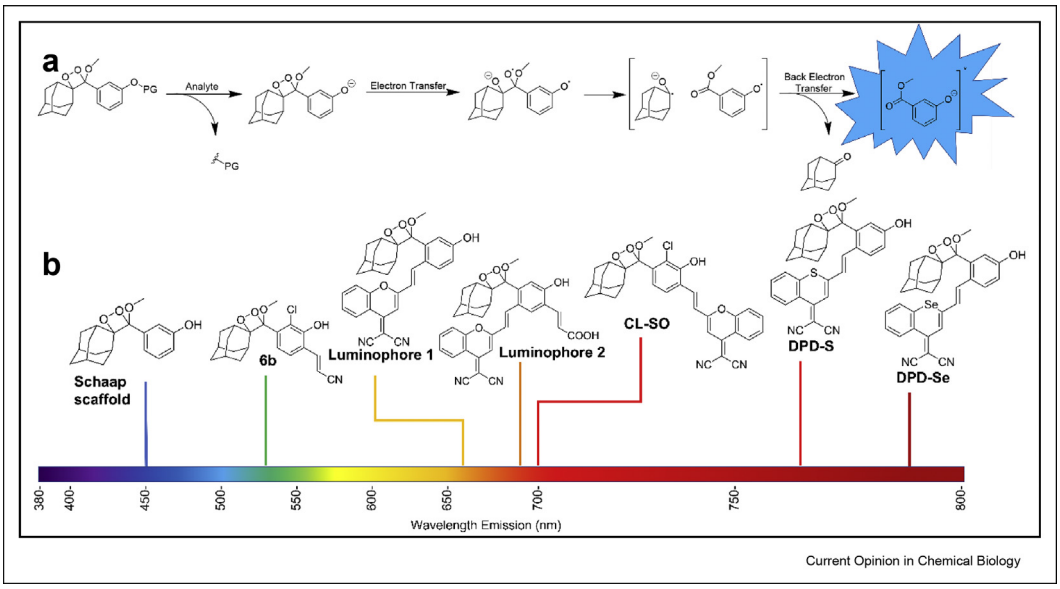

(**a**) General scheme of CIEEL mechanism (**b**) Structural evolution of spiroadamantane-1,2-dioxetanes towards near-infrared emission.

signal decay, number of replicates and units of chemiluminescence measurement, which are important in interpreting analytical outcomes.

Imaging of small molecules and ions

Ions and reactive oxygen, nitrogen, and sulfur species are integral endogenous signaling molecules that orchestrate cellular health, but disruptions in a cell's health can result in pathological perturbations of endogenous levels [18]. Simple, yet elegant modifications of either the caging group or the dioxetane scaffold can lead to the detection of a variety of small molecules. For example, our lab designed a ratiometric pH probe **Ratio-pHCL-1** (Figure 2a), composed of a pH-sensitive carbofluorescein attached to the 1,2-dioxetane scaffold [19]. With its red shifted emission of 580 nm and accurate pH measurements from 6.8 to 8.4, it provides excellent *in vivo* IVIS images of intraperitoneal (IP) injections in BALB-C mice with high photon flux. Another instance of ion sensing included the utilization of a *tert*-butyldimethylsilyl (TBS) protecting group that could be selectively removed by fluoride ions [20]. This probe **CL-F** was consequently employed for imaging fluoride ions in a BALB-C mouse. Small molecule imaging can be extended to foreign contaminants as well. Li and co-workers [21] developed a chemiluminescent palladium (II) ion probe **PCL** (Figure 2b) with a Pd-cleavable butynyl moiety which afforded high sensitivity and selectivity (with 20% v/v Emerald II Enhancer) to traces of palladium. Moreover, its aqueous stability allowed *in vivo* imaging within a mouse. Li and co-workers also designed an H_2S probe comprised of a 2,4-dinitrophenyl caged 1,2-dioxetane **SCL-2** [22]. This afforded imaging of H_2S (using NaHS) in BALB-C mice intraperitoneally. Interestingly, a slight modification of the caging group to include a 2,4-dinitrophenylsulfonyl group gave a probe **SHCL** (Figure 2c) that allowed imaging of biothiols like glutathione both exogenously and endogenously in nude mice [23]. Two reactive nitrogen species that have been targeted include azanone (HNO) and peroxynitrite ($ONOO^-$). In 2019, our lab reported a real-time HNO monitoring probe **HNOCL-1** (Figure 2d) by appending a triaryl phosphine group to the 1,2-dioxetane scaffold [24]. This work is noteworthy because the kinetics of the chemiluminescence response was solved and used to achieve precise quantification of HNO in real-time with temporal precision similar to an HNO electrode. When imaged in a BALB-C mouse via IP injection of **HNOCL-1** treated with Angeli's salt, a 300-fold increase in chemiluminescence was observed when compared to a control over the course of 30 min.

An example of hypoxia imaging was demonstrated by our group by developing the probe **HyCL-4-AM** (Figure 2e) [25]. Containing a nitroaromatic sensing moiety and, importantly, an acetoxymethyl (AM) ester, this probe performs dramatically well in cells and animals, where quantitative information on oxygen-dependent intracellular enzyme kinetics could be attained. For efficient monitoring of HOCl generation, Cui and co-workers developed a dioxetane probe **CL-N** containing a 4-aminophenyl cage which enabled *in vivo* HOCl imaging both exogenously and in tumors [26]. Another approach involved the use of an electron rich 2,6-dichlorophenol cage, where the probe **HOCl-CL-510** was able to detect HOCl in live mice exogenously, via lipopolysaccharide (LPS) stimulation, and in an arthritic mice model [27]. In another example, Li and

Figure 2

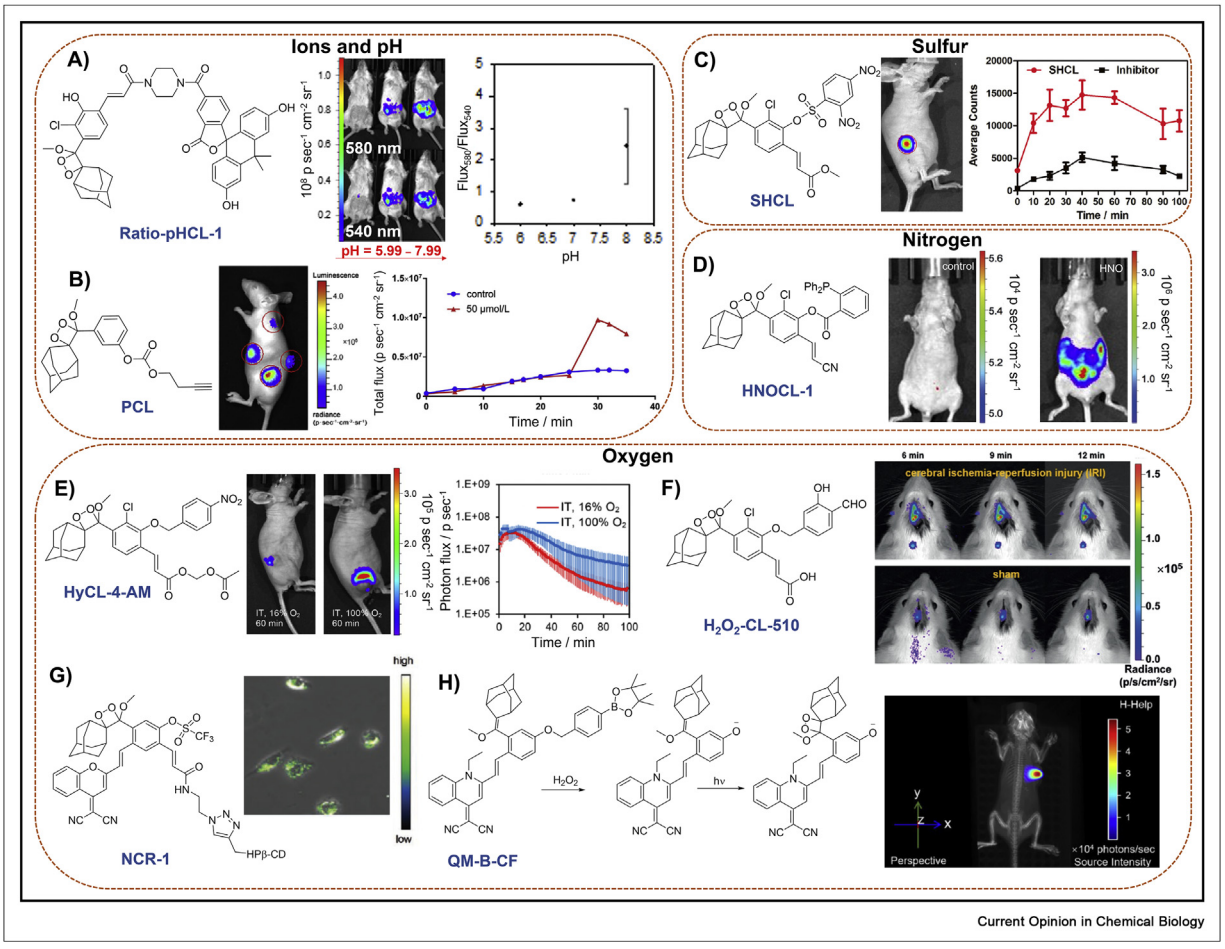

Representative chemiluminescent spiroadamantane-1,2-dioxetane probes used for *in vivo* and cellular imaging of small molecules and ions. (**a**) Ratiometric pH imaging via energy transfer. Adapted with permission from Ref. [19]. Copyright 2020 American Chemical Society. (**b**) Butynyl appended probe used for the detection of palladium (II) ions. Adapted with permission from Ref. [21]. Copyright 2019 Elsevier. (**c**) Biothiol detection via a 2,4-dinitrophenylsulfonyl caged acrylate scaffold. Adapted with permission from Ref. [23]. Copyright 2021 Elsevier. (**d**) Triarylphosphine-caged acrylonitrile scaffold used for detection and precise quantification of azanone, (HNO) via kinetic analyses. Adapted with permission from Ref. [24]. Copyright 2019 John Wiley and Sons. (**e**) Hypoxia detection in tumors via a 4-nitrobenzyl-caged acetoxymethyl ester modified scaffold. Adapted with permission from Ref. [25]. Copyright 2019 American Chemical Society. (**f**) Salicylaldehyde-caged acrylic acid probe used for detection of ischemia-reperfusion injury induced H_2O_2. Adapted with permission from Ref. [30]. Copyright 2020 John Wiley and Sons. (**g**) Trifluoromethanesulfonate-caged *p*-dicyanomethylene-4H-pyran containing scaffold used for detection of superoxide ($O_2^{\bullet-}$). Adapted with permission from Ref. [31]. Copyright 2020 John Wiley and Sons. (**h**) Dual fluorescence-chemiluminescence detection of H_2O_2 via a quinoline-malononitrile modified scaffold caged with an aryl boronate trigger. Adapted with permission from Ref. [32]. Copyright 2020 John Wiley and Sons.

co-workers reported several thiocarbamate-caged HOCl probes, where the acrylic acid functionalized probe **HCCL-2** demonstrated real-time HOCl detection in live mice via LPS stimulation [28]. Using a boronate-protected dioxetane probe **H_2O_2-CL**, Caliceti and co-workers were able to demonstrate chemiluminescence microscopy of H_2O_2 in human living cells (Caco-2) which had been treated with menadione to induce H_2O_2 production [29]. The cellular images were obtained using an Olympus IX73 inverted microscope, equipped with a 10× objective and an EM-CCD camera (ImagEM X2), with 5 min exposure times. This work is also noteworthy as it provides a careful validation of the probe in cellular models of inflammation. An alternate strategy involved the utilization of a salicylaldehyde cage, allowing the resulting probe **H_2O_2-CL-510** to monitor of ischemia-reperfusion injury induced H_2O_2 changes *in vivo* (Figure 2f) [30].

To monitor the species produced during drug-induced acute kidney injury, Pu and co-workers developed two chemiluminescent probes containing a *p*-dicyanomethylene-4H-pyran unit with the phenol caged with either trifluoromethanesulfonate (**NCR1**, for superoxide $O_2^{\bullet-}$, Figure 2g) or formate (**NCR2**, for $ONOO^-$) [31]. Chemiluminescence microscopy of cisplatin-

Figure 3

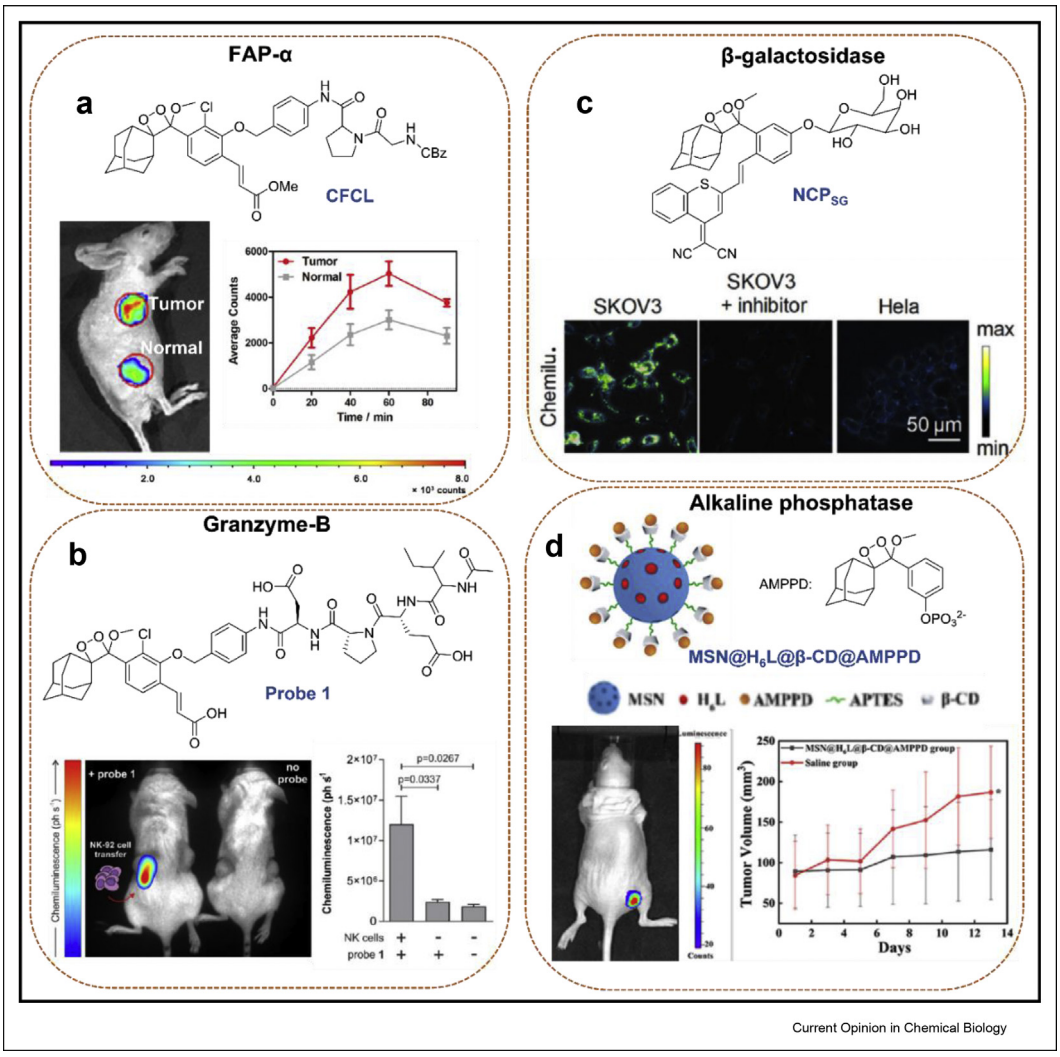

Chemiluminescent probes used for *in vivo* and cellular imaging of enzyme activity. (**a**) Detection of endogenous fibroblast activation protein α (FAP-α) in tumors via a FAP-α cleavable dipeptide sequence. Adapted with permission from Ref. [38]. Copyright 2021 American Chemical Society. (**b**) Detection of anti-tumor activity of NK cells via a granzyme-B specific trigger. Adapted with permission from Ref. [39]. Copyright 2021 John Wiley and Sons. (**c**) Near-infrared detection of β-galactosidase in cancer cells using a galactose-caged thiopyran modified scaffold. Adapted with permission from Ref. [40]. Copyright 2021 John Wiley and Sons. (**d**) Nanoparticle probe used in detection of alkaline phosphatase in tumors, as well as in the inhibition of tumor growth. Adapted with permission from Ref. [41]. Copyright 2021 American Chemical Society.

treated proximal tubule epithelial human kidney 2 (HK2) cells and *in vivo* chemiluminescence kidney imaging of mice treated with cisplatin established the ability of both probes to detect the respective reactive species at different post-drug treatment times. By further modifying the dicyanomethylene-4H-pyran to a quinoline-malononitrile unit and using an aryl boronate trigger, Guo and co-workers developed an H_2O_2 sensitive probe **QM-B-CF** (Figure 2h) that operates via a 'dual-lock strategy' [32]. Analyte-triggered accumulation of a stable pre-chemiluminescent moiety led to an aggregation-induced emission (AIE), and consequent photooxidation of the moiety gave the 1,2-dioxetane, which generates the chemiluminescent signal upon decomposition. This dual luminescence was exploited to detect intratumoral H_2O_2 in live mice under both fluorescence and chemiluminescence (after 2 min white laser irradiation) modes, where a 66-fold higher chemiluminescence signal was obtained for the latter compared to luminol. A similar technique could be envisioned with other types of photoactivatable and photoswitchable chemiluminescent probes [33]. A related approach was used for singlet oxygen detection by Fan and co-workers where the dioxetane was generated *in situ* from the precursor probe **CL-SO** with the help of a $^1O_2$ evolving H_2O_2/NaClO system or in the

presence of a photosensitizer and irradiation [34]. This allowed imaging of both $^1O_2$ and photodynamic therapy actions (12 min irradiation time) in live mice. Another strategy for NIR imaging was adopted by Li and co-workers where they attached two acyl-protected dioxetane scaffolds to a red-emitting AIEgen fluorophore [35]. This energy transfer-based chemiluminescent probe **ACLD** was then utilized for exogenous imaging of hydrazine in BALB/c mice.

Chemiluminescent probes have also been utilized for multi-biomarker detection, an exciting prospect which can assist in establishing biomarker correlation and improving diagnostic capabilities. In 2019, Pu and co-workers developed a chemo-fluoro-luminescent reporter (**CFR**) for the sequential detection of $O_2^{\bullet-}$ (oxidative stress) and caspase-3 (cellular apoptosis) generated during drug-induced hepatotoxicity in live mice [36]. The probe consists of a trifluoromethanesulfonate-caged phenol dioxetane appended to a fluorescent hemicyanine unit caged with a caspase-3 cleavable peptide modified self-immolative linker. This afforded independent chemiluminescent and near-infrared fluorescent channels which allowed early biomarker detection (17.5 h earlier than histological analysis for $O_2^{\bullet-}$). The same group also reported a renal clearable dual channel probe $\mathbf{MRP_D}$ which is always fluorescent but exhibits chemiluminescence only in the presence of $O_2^{\bullet-}$, allowing dual chemiluminescence-fluorescence imaging of cisplatin-induced acute kidney injury in live mice [37].

Imaging of enzyme activity

Enzymes act as important biomarkers as their activity and the relative concentrations are indicative of cell function. Recently, the first chemiluminescent probe **CFCL** (Figure 3a) for detection of endogenous fibroblast activation protein α (FAP-α) was developed by utilizing a FAP-α specific dipeptide substrate cage [38].

Figure 4

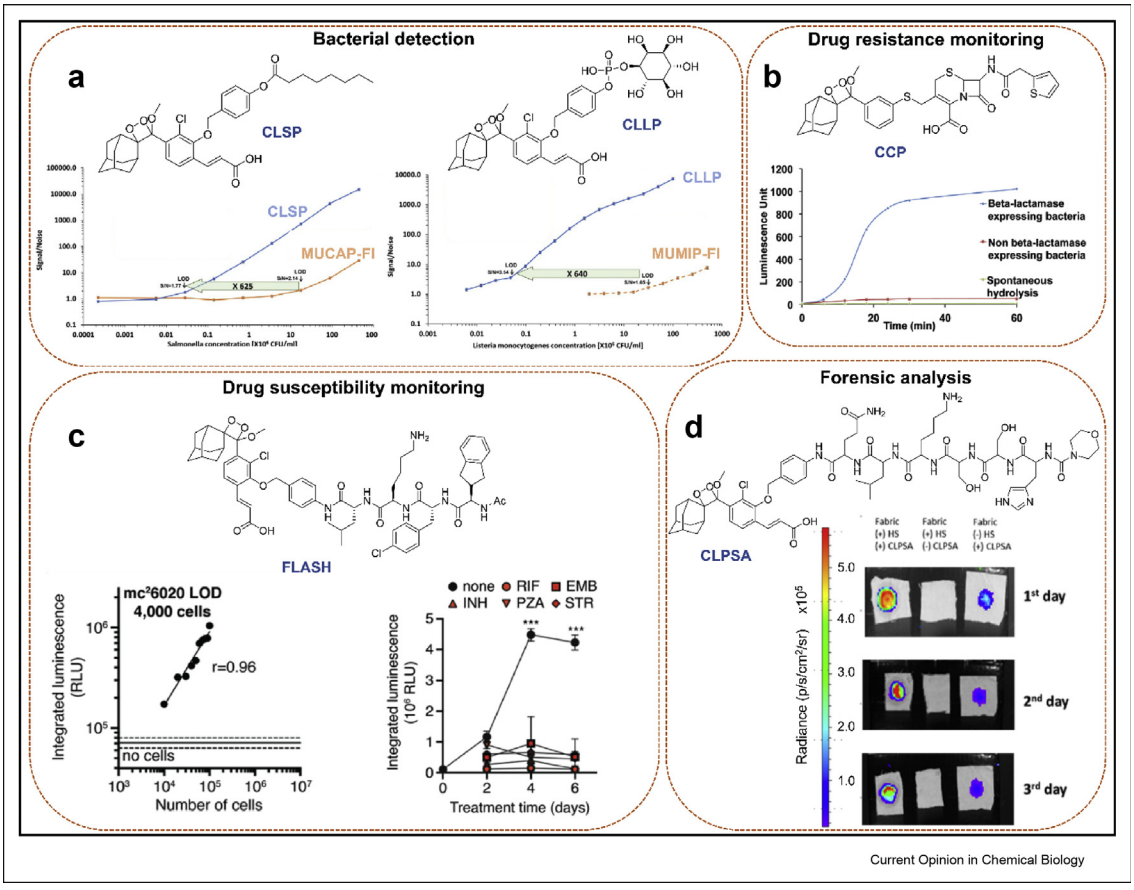

Chemiluminescence-based disease monitoring and forensic applications. (**a**) Detection of *Salmonella* esterase or for *Listeria monocytogenes* phospholipase. Adapted with permission from Ref. [42]. Copyright 2019 John Wiley and Sons. (**b**) Monitoring of β-lactamase expressing bacteria. Adapted with permission from Ref. [44]. Copyright 2020 The Royal Society of Chemistry. (**c**) Tracking the susceptibility of *Mycobacterium tuberculosis* towards antibacterial drugs. Adapted with permission from Ref. [45]. Copyright 2021 American Chemical Society. (**d**) Forensic detection of human semen. Adapted with permission from Ref. [46]. Copyright 2020 American Chemical Society.

Table 1

Summary of chemiluminescent probes discussed in this review.

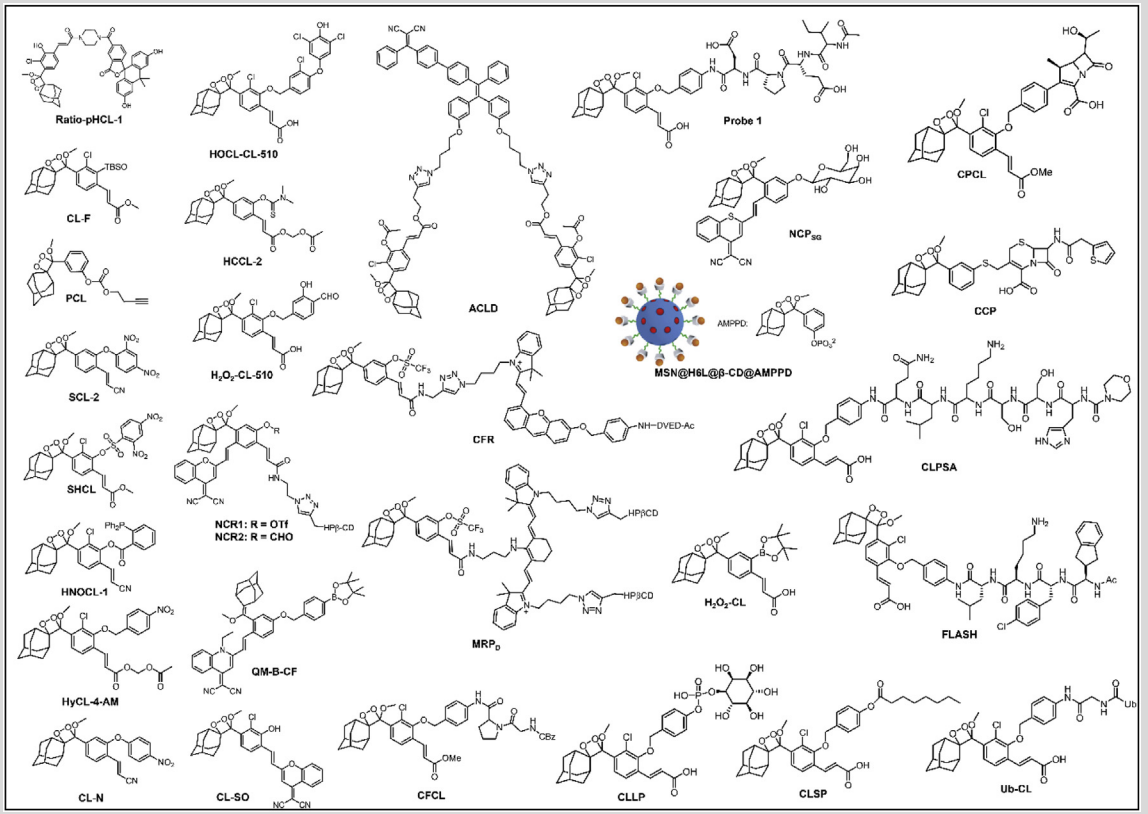

Animal imaging

Probe	λ_{CL} (nm)	Analyte	Mice, Injection	Peak Brightness[a]	Trials	Time Course	Ref
Ratio-pHCL-1	530, 580	pH	BALB-C, IP	1×10^8 p s^{-1} cm^{-2} sr^{-1}	3	Single	[19]
CL-F	540	F^-	BALB-C, back injection	Arbitrary units	2	Single	[20]
PCL	450–470	Pd^{2+}	Subcutaneous	4.5×10^7 p s^{-1} cm^{-2} sr^{-1}	3	35 min	[21]
SCL-2	450–470	H_2S	BALB-C, IP	2.5×10^7 p s^{-1} cm^{-2} sr^{-1}	3	60-min	[22]
SHCL	540	biothiols	Subcutaneous	1.5×10^5 p s^{-1} cm^{-2} sr^{-1}	3	Single	[23]
HNOCL-1	525	HNO	BALB-C, IP	3.6×10^6 p s^{-1} cm^{-2} sr^{-1}	1	30-min	[24]
HyCL-4-AM	516	Hypoxia in tumors	IM, IP	10^5 p s^{-1} cm^{-2} sr^{-1}	3–6	100-min	[25]
CL-N	525	HOCl	BALB-C, IP, IT	Signal/noise ratios	1	60-min (IP) 80-min (IT)	[26]

HOCL-CL-510	520–540	HOCl	Subcutaneous, IP, tibiotarsal joint	10^6 p s^{-1} cm^{-2} sr^{-1}	1	30-min (Sub) 21-min (IP) 12-min (TibJ)	[27]
HCCL-2	520–540	HOCl	BALB-C, IP	1.3×10^8 p s^{-1} cm^{-2} sr^{-1}	3	10 min	[28]
H_2O_2-CL-510	520–540	H_2O_2	Live rat, brain ventricle	10^5 p s^{-1} cm^{-2} sr^{-1}	3	12 min	[30]
NCR1, NCR2	700	$O_2^{\bullet-}$, $ONOO^-$	Live mice, IV	13×10^6 p s^{-1} cm^{-2} sr^{-1}	3	60–120 min	[31]
QM-B-CF	600	H_2O_2	Live mice, IT	5.6×10^5 p s^{-1} cm^{-2} sr^{-1}	1	120-min	[32]
CL-SO	700	$^1O_2$	BALA-C, IP	17500 cps	2	12-min	[34]
ACLD	620	N_2H_4	BALB-C, skin-pop	Arbitrary units	1	80-min	[35]
CFR	540	$O_2^{\bullet-}$	IV	6×10^4 p s^{-1} cm^{-2} sr^{-1}	3	120 min	[36]
MRP_D	540	$O_2^{\bullet-}$	IV	4.8×10^4 p s^{-1} cm^{-2} sr^{-1}	3	120 min	[37]
CFCL	550	FAP-α	BALB-C, IV, IT	10^6 p s^{-1} cm^{-2} sr^{-1}	1	60-min 110-min	[38]
Probe 1	520–540	Granzyme-B	IT	1.5×10^7 p s^{-1}	3	–	[39]
NCP_{SG}	>750	β-galactosidase	IT	10^4 p s^{-1} cm^{-2} sr^{-1}	3	60-min	[40]
MSN@H6L@β-CD@AMPPD	660	Alkaline phosphatase	IV	90 Arbitrary units	5	60-min	[41]

Chemiluminescence microscopy

Probe	λ_{CL} (nm)	Analyte	Cell Type	Instrumentation	Acquisition time (s)	Ref
H_2O_2-CL	540	H_2O_2	Caco-2	Olympus IX73 inverted microscope, EM-CCD camera	5	[29]
NCR1, NCR2	700	$O_2^{\bullet-}$, $ONOO^-$	HK2	LX71 inverted microscope, infinity 3-1 (Lumenera) CCD camera	10	[31]
NCP_{SG}	>750	β-galactosidase	SKOV3	LX71 inverted microscope, infinity 3-1 (Lumenera) CCD camera	60	[40]

Monitoring disease and infection

Probe	λ_{CL} (nm)	Enzyme detected	Signal intensity	Ref
CLSP	520–540	Esterase–*Salmonella*	1.6×10^7 RLU	[42]
CLLP	520–540	Phospholipase–*Listeria Monocytogenesis*	1.0×10^6 RLU	[42]
CPCL	540	Carbapenemase–*Imipenem-resistant Pseudomonas aeruginosa and Klebsiella pneumoniae*	40000 RLU	[43]
CCP	470	β-lactamase–*E. Coli*	1000 LU	[44]
FLASH	520–540	Hip-1–*Mycobacterium tuberculosis*	2.5×10^5 RLU	[45]
CLPSA	520–540	Prostate specific antigen–Human semen	~20000 RLU	[46]
Ub-CL	520–540	Deubiquitinating enzymes	180000 RLU	[47]

[a] Highest pixel intensity in image.

Successful *in vivo* imaging was achieved via both intravenous and intratumoral injections, and the probe demonstrates the ability to distinguish between different microenvironments on the same mouse (tumor vs normal). Similarly, *in vivo* chemiluminescent monitoring of the anti-tumor activity of natural killer (NK) cells was achieved by deploying a dioxetane probe with a Granzyme-B specific peptide sequence (Figure 3b) [39]. Through intratumoral studies, the ability of the probe to distinguish between NK cells-treated and untreated tumors was established in live mice. In 2021, Pu and co-workers developed new chemiluminescent probes by replacing the oxygen atom on a dicyanomethylene-4H-pyran unit by a larger sulfur (**NCP_s**) or selenium (**NCP_{Se}**) atom, leading to emission wavelengths greater than 750 nm [40]. Importantly, chemiluminescence microscopy of cells was established using a galactose-caged thiopyran probe **NCP_{SG}** (Figure 3c), which provided better discrimination of β-gal cells than the corresponding fluorescence signals. The authors were also able to achieve intratumoral *in vivo* imaging in SKOV3 (β-gal positive) or HeLa tumor (β-gal negative) bearing nude mice, where a 6.5-fold increase in chemiluminescence signal was observed from the SKOV3 tumor in comparison to the HeLa tumor. An interesting chemiluminescent nanoparticle-based approach was adopted by Tang, Li and co-workers to address liver cancer theranostics [41]. Using a building-block approach, the probe, **MSN@H_6L@β-CD@AMPPD** was developed by covalently attaching a phosphate-caged 1,2-dioxetane (AMPPD)-β-cyclodextrin adduct to a biocompatible mesoporous silica nanoparticle via a (4-carboxyphenyl) porphyrin linker (Figure 3d). Showing specificity for alkaline phosphatase (ALP), the nanoparticle probe demonstrated NIR chemiluminescence via energy transfer from AMPPD to the porphyrin. The specificity of the probe was further reflected in the *in vivo* trials where tumor localization was observed upon intravenous injection, with the brightest signal occurring at 30 min over a 60 min time course. Furthermore, its therapeutic ability via $^1O_2$ generation was assessed by monitoring cell viability (cancer vs normal cells), as well as tumor growth in live mice. From both studies it was evident that the nanoparticle probe selectively kills cancer cells and inhibits tumor growth, which is an exciting prospect for chemiluminescence-based photodynamic therapy.

Applications for monitoring disease and infection

While the above examples demonstrate the imaging capabilities of 1,2-dioxetanes, the high sensitivity of these probes also show remarkable potential for clinical monitoring, detecting bacterial infection/contamination, and forensics. It should be noted that these 'non-imaging' probes are able to monitor microbial infections via detection of enzyme activity. In 2019, the probes **CLSP** and **CLLP** (Figure 4a) were reported, bearing substrates specific for *Salmonella* esterase or for *Listeria monocytogenes* phospholipase, respectively [42]. These probes were able to detect the specific bacteria with limits of detection that were about 600-fold lower than the corresponding fluorescent probes and could detect *Salmonella* within a 6-h incubation period. Apart from detection, chemiluminescent probes have also been used for drug resistance monitoring. For instance, Shabat, Spitz and co-workers developed the first carbapenemase-specific chemiluminescent probe **CPCL** for the detection of live carbapenemase-producing organisms, which can develop antibiotic resistance to carbapenem-based drugs [43]. A related β-lactamase detecting probe was developed by Murthy and co-workers [44]. This probe **CCP** was synthetically unique since it consists of cephalosporin conjugated to a thiol rather than the commonly used phenol derivates (Figure 4b). Highlights of this probe include increased sensitivity (4-fold magnitude) compared to the commercial fluorescent probe Fluorocillin, and the ability to selectively detect β-lactamase activity in cultural and clinical bacterial isolates. Similarly, Bogyo and co-workers devised a chemiluminescent probe, **FLASH** (Figure 4c) which is specific for the *Mycobacterium tuberculosis* (Mtb) protease Hip1 [45]. While detecting as few as thousands of live Mtb cells in both culture and human sputum samples within minutes, **FLASH** was able to differentiate between dead and live bacteria, as well as between antibiotic-susceptible and resistant strains. These examples showcase the ability of chemiluminescent probes to provide fast and sensitive diagnosis of deadly microbes, as well as provide opportunities to improve antibacterial therapeutics.

The forensic applicability of such probes has also been investigated. In 2020, Shabat and co-workers attached a prostate specific antigen (PSA) peptidyl substrate Mu-HSSKLQ to the dioxetane scaffold [46]. The resulting probe **CLPSA** (Figure 4d) was employed for the detection of seminal fluid at low dilutions (1:31250) using a portable chemiluminescence luminometer (Lumini). Importantly, **CLPSA** was able to detect human semen traces deposited on fabric even after 3 days, with radiance in the range of 10^5 p s^{-1} cm^{-2} sr^{-1}. Another example involved the direct attachment of a protein, ubiquitin to yield the first protein-dioxetane luminophore conjugate [47]. This probe, **Ub-CL** could determine the activity of deubiquitinating enzymes (DUBs) which serve as markers for human diseases like cancer. Significantly, higher signal-to-noise ratios (>93-fold) were obtained for this chemiluminescent probe in comparison to the commercially available fluorescent probe Ub-AMC (1.5-fold).

Conclusions

Tremendous advances for live animal chemiluminescence imaging have been made over the last few years, with a plethora of probes being developed for

imaging of small molecules and enzyme activity. Moreover, chemiluminescent probes have also been demonstrated as potential diagnostic and theranostic tools for disease and infection. From the reports discussed above, key observations can be made. First, targeted injections seem to perform better than IV injections. While targeted injections can be very useful for spatially and temporally resolved imaging in known tissue sites, they are not suitable for identifying unknown sites of disease like cancer metastases, for example. It is envisioned that advanced triggers with high selectivity or well-resolved ratiometric/kinetics-based methods may enhance chemiluminescence imaging with systemic IV injections and could be a fruitful avenue for future investigation. In addition, investigating the time course of the signal change can be highly informative, as it can unveil kinetic trends. Equally important is the number of replicates which help elucidate reproducibility and provide a more accurate portrayal of each probe's behavior. Table 1 summarizes the imaging studies of probes discussed in this study, with an emphasis on injection type, brightness, replicates, and kinetics. There is a need for real-time quantification of analytes using ratiometric and kinetics-based methods [19,25], and we envision an increased employment of such methodologies soon. Combining chemiluminescent small molecule probes with chemical biological systems such as split esterases [48] and deoxyribozymes [49] are some other fascinating avenues with potential applications in signaling and synthetic biology and need more exploring. Lastly, in comparison to animal imaging, examples of chemiluminescence microscopy are rare due in part to a need for instrumentation and methods optimized for chemiluminescence microscopy [29,31,40,50–53]. Overall, the future holds promise and exciting prospects for chemiluminescence-based imaging.

Declaration of competing interest

The authors declare the following financial interests/personal relationships which may be considered as potential competing interests: Alexander R. Lippert reports a relationship with BioLum Sciences, LLC that includes: equity or stocks.

Acknowledgements

Funding from the National Science Foundation (CHE 1653474) and the National Institutes of Health (R15GM114792-02) are gratefully acknowledged.

References

Papers of particular interest, published within the period of review, have been highlighted as:

* of special interest
** of outstanding interest

1. Yang M, Huang J, Fan J, *et al.*: **Chemiluminescence for bioimaging and therapeutics: recent advances and challenges**. *Chem Soc Rev* 2020, **49**:6800–6815.

2. Zhan Z, Dai Y, Li Q, Lv Y: **Small molecule-based bioluminescence and chemiluminescence probes for sensing and imaging of reactive species**. *Trends Anal Chem* 2021, **134**:116129.

3. Wu L, Sedgwick AC, Sun X, *et al.*: **Reaction-based fluorescent probes for the detection and imaging of reactive oxygen, nitrogen, and sulfur species**. *Acc Chem Res* 2019, **52**:2582–2597.

4. Bezner BJ, Ryan LS, Lippert AR: **Reaction-based luminescent probes for reactive sulfur, oxygen, and nitrogen species: analytical techniques and recent progress**. *Anal Chem* 2020, **92**:309–326.

5. Yang Y, Zhang F: **Activatable Chemiluminescent molecular probes for bioimaging and biosensing**. *Anal Sens* 2021, **1**:75–89.

6. Schaap AP, Handley RS, Giri BP: **Chemical and enzymatic triggering of 1,2-dioxetanes. 1: aryl esterase-catalyzed chemiluminescence from a naphthyl acetate-substituted dioxetane**. *Tetrahedron Lett* 1987, **28**:935–938.

7. Schaap AP, Chen T-S, Handley RS, *et al.*: **Chemical and enzymatic triggering of 1,2-dioxetanes. 2: fluoride-induced chemiluminescence from tert-butyldimethylsilyloxy-substituted dioxetanes**. *Tetrahedron Lett* 1987, **28**:1155–1158.

8. Schaap AP, Sandison MD, Handley RS: **Chemical and enzymatic triggering of 1,2-dioxetanes. 3: alkaline phosphatase-catalyzed chemiluminescence from an aryl phosphate-substituted dioxetane**. *Tetrahedron Lett* 1987, **28**:1159–1162.

9. Hananya N, Shabat D: **Recent advances and challenges in luminescent imaging: bright outlook for chemiluminescence of dioxetanes in water**. *ACS Cent Sci* 2019, **5**:949–959.

10. Adam W, Bronstein I, Trofimov AV, Vasil'ev RF: **Solvent-cage effect (viscosity dependence) as a diagnostic probe for the mechanism of the intramolecular chemically initiated electron-exchange luminescence (CIEEL) triggered from a spiroadamantyl-substituted dioxetane**. *J Am Chem Soc* 1999, **121**:958–961.

11. Ciscato LFML, Bartoloni FH, Weiss D, *et al.*: **Experimental evidence of the occurrence of intramolecular electron transfer in catalyzed 1,2-dioxetane decomposition**. *J Org Chem* 2010, **75**:6574–6580.

12. Catalani LH, Wilson T: **Electron transfer and chemiluminescence. Two inefficient systems: 1,4-dimethoxy-9,10-diphenylanthracene peroxide and diphenoyl peroxide**. *J Am Chem Soc* 1989, **111**:2633–2639.

13. Cui D, Li J, Zhao X, *et al.*: **Semiconducting polymer nanoreporters for near-infrared chemiluminescence imaging of immunoactivation**. *Adv Mater* 2020, **32**:1906314.

14. Gnaim S, Scomparin A, Eldar-Boock A, *et al.*: **Light emission enhancement by supramolecular complexation of chemiluminescence probes designed for bioimaging**. *Chem Sci* 2019, **10**:2945–2955.

15. Green O, Gnaim S, Blau R, *et al.*: **Near-infrared dioxetane luminophores with direct chemiluminescence emission mode**. *J Am Chem Soc* 2017, **139**:13243–13248.

16. Hananya N, Eldar Boock A, Bauer CR, *et al.*: **Remarkable enhancement of chemiluminescent signal by dioxetane–fluorophore conjugates: TURN_ON chemiluminescence probes with color modulation for sensing and imaging**. *J Am Chem Soc* 2016, **138**:13438–13446.

17. Haris U, Kagalwala HN, Kim YL, Lippert AR: **Seeking illumination: the path to chemiluminescent 1,2-dioxetanes for quantitative measurements and in vivo imaging**. *Acc Chem Res* 2021, **54**:2844–2857.

18. Li B, Kim YL, Lippert AR: **Chemiluminescence measurement of reactive sulfur and nitrogen species**. *Antioxidants Redox Signal* 2021, https://doi.org/10.1089/ars.2021.0195.

19. ** Ryan LS, Gerberich J, Haris U, *et al.*: **Ratiometric pH imaging using a 1,2-dioxetane chemiluminescence resonance energy transfer sensor in live animals**. *ACS Sens* 2020, **5**:2925–2932.
Describes a single molecule 1,2-dioxetane, ratiometric, chemiluminescent probe to detect pH in live animals. Through CIEEL and a

chemiluminescence resonance energy transfer (CRET) mechanism, this probe provides accurate pH measurements from 6.8–8.4. Its ratiometric properties allow its emission to be independent of confounding variables.

20. Gu B, Dong C, Shen R, *et al.*: **Dioxetane-based chemiluminescent probe for fluoride ion-sensing in aqueous solution and living imaging**. *Sensor Actuator B Chem* 2019, **301**:127111.

21. Gao Y, Lin Y, Liu T, *et al.*: **A specific and selective chemiluminescent probe for Pd^{2+} detection**. *Chin Chem Lett* 2019, **30**:63–66.

22. Zhang Z, Lin Y, Li Z, *et al.*: **Bright chemiluminescent dioxetane probes for the detection of gaseous transmitter H_2S**. *Bioorg Med Chem Lett* 2021, **46**:128148.

23. Fu A, Mao Y, Wang H, Cao Z: **An activatable chemiluminescence probe based on phenoxy-dioxetane scaffold for biothiol imaging in living systems**. *J Pharm Biomed* 2021, **204**:114266.

24. An W, Ryan LS, Reeves AG, *et al.*: **A chemiluminescent probe for HNO quantification and real-time monitoring in living cells**. *Angew Chem Int Ed* 2019, **58**:1361–1365.

25. Ryan LS, Gerberich J, Cao J, *et al.*: **Kinetics-based measurement of hypoxia in living cells and animals using an acetoxymethyl ester chemiluminescent probe**. *ACS Sens* 2019, **4**:1391–1398.

26. Wang C, Wang T, Zhang M, *et al.*: **Chemiluminescence molecular sensor for endogenous HOCl in vivo**. *Sensor Actuator B Chem* 2021, **339**:129927.

27. ** Ye S, Yang B, Wu M, *et al.*: **Recurring real-time monitoring of inflammations in living mice with a chemiluminescent probe for hypochlorous acid**. *CCS Chem* 2021:2181–2188.
Describes a highly selective and sensitive 1,2-dioxetane probe for sensing HOCl both *in vivo* and *in vitro*. This probe can achieve real-time monitoring in both acute and chronic inflammation models of living mice, providing a valuable tool for the imaging of HOCl related diseases.

28. Sun Y, Gao Y, Tang C, *et al.*: **Multiple rapid-responsive probes towards hypochlorite detection based on dioxetane luminophore derivatives**. *J Pharm Anal* 2021, https://doi.org/10.1016/j.jpha.2021.10.001.

29. * Calabria D, Guardigli M, Mirasoli M, *et al.*: **Selective chemiluminescent TURN-ON quantitative bioassay and imaging of intracellular hydrogen peroxide in human living cells**. *Anal Biochem* 2020, **600**:113760.
Depicts a chemiluminescent 1,2-dioxetane bioassay for the quantification of H_2O_2 in living cells, which provides one of the fastest incubation times used in a luminescence-based bioassay. Careful validation and chemiluminescence microscopy provide valuable insight.

30. Ye S, Hananya N, Green O, *et al.*: **A highly selective and sensitive chemiluminescent probe for real-time monitoring of hydrogen peroxide in cells and animals**. *Angew Chem Int Ed* 2020, **59**:14326–14330.

31. * Huang J, Huang J, Cheng P, *et al.*: **Near-infrared chemiluminescent reporters for in vivo imaging of reactive oxygen and nitrogen species in kidneys**. *Adv Funct Mater* 2020, **30**:2003628.
Depicts two NIR 1,2-dioxetane probes which can detect real-time images of reactive oxygen and nitrogen species. Their red-shifted NIR emission allows for deeper tissue penetration, making them more applicable to biological imaging through tissue.

32. Zhang Y, Yan C, Wang C, *et al.*: **A sequential dual-lock strategy for photoactivatable chemiluminescent probes enabling bright duplex optical imaging**. *Angew Chem Int Ed* 2020, **59**:9059–9066.

33. Ryan LS, Nakatsuka A, Lippert AR: **Photoactivatable 1,2-dioxetane chemiluminophores**. *Res Chem* 2021, **3**:100106.

34. Yang M, Zhang J, Shabat D, *et al.*: **Near-infrared chemiluminescent probe for real-time monitoring singlet oxygen in cells and mice model**. *ACS Sens* 2020, **5**:3158–3164.

35. Li J, Hu Y, Li Z, *et al.*: **Photoactivatable red chemiluminescent AIEgen probe for in vitro/vivo imaging assay of hydrazine**. *Anal Chem* 2021, **93**:10601–10610.

36. Cheng P, Miao Q, Li J, *et al.*: **Unimolecular chemo-fluoro-luminescent reporter for crosstalk-free duplex imaging of hepatotoxicity**. *J Am Chem Soc* 2019, **141**:10581–10584.

37. Huang J, Li J, Lyu Y, *et al.*: **Molecular optical imaging probes for early diagnosis of drug-induced acute kidney injury**. *Nat Mater* 2019, **18**:1133–1143.

38. Fu A, Wang H, Huo T, *et al.*: **A novel chemiluminescence probe for sensitive detection of fibroblast activation protein-alpha in vitro and in living systems**. *Anal Chem* 2021, **93**:6501–6507.

39. Scott JI, Gutkin S, Green O, *et al.*: **A functional chemiluminescent probe for in vivo imaging of natural killer cell activity against tumours**. *Angew Chem Int Ed* 2021, **60**:5699–5703.

40. ** Huang J, Jiang Y, Li J, *et al.*: **Molecular chemiluminescent probes with a very long near-infrared emission wavelength for in vivo imaging**. *Angew Chem Int Ed* 2021, **60**:3999–4003.
Describes 1,2-dioxetane chemiluminescent probes with record long NIR emissions, allowing them to be much more applicable for biological imaging through tissue. Caging with galactose gave a highly selective and sensitive probe **NCP_{SG}** for the enzyme detection of β-galactosidase within cells and *in vivo*.

41. Fan N, Li P, Wu C, *et al.*: **ALP-activated chemiluminescence PDT nano-platform for liver cancer-specific theranostics**. *ACS Appl Bio Mater* 2021, **4**:1740–1748.

42. Roth-Konforti M, Green O, Hupfeld M, *et al.*: **Ultrasensitive detection of salmonella and listeria monocytogenes by small-molecule chemiluminescence probes**. *Angew Chem Int Ed* 2019, **58**:10361–10367.

43. Das S, Ihssen J, Wick L, *et al.*: **Chemiluminescent carbapenem-based molecular probe for detection of carbapenemase activity in live bacteria**. *Chem Eur J* 2020, **26**:3647–3652.

44. Maity S, Wang X, Das S, *et al.*: **A cephalosporin–chemiluminescent conjugate increases beta-lactamase detection sensitivity by four orders of magnitude**. *Chem Commun* 2020, **56**:3516–3519.

45. Babin BM, Fernandez-Cuervo G, Sheng J, *et al.*: **Chemiluminescent protease probe for rapid, sensitive, and inexpensive detection of live Mycobacterium tuberculosis**. *ACS Cent Sci* 2021, **7**:803–814.

46. Gutkin S, Green O, Raviv G, *et al.*: **Powerful chemiluminescence probe for rapid detection of prostate specific antigen proteolytic activity: forensic identification of human semen**. *Bioconjugate Chem* 2020, **31**:2488–2493.

47. Gutkin S, Gandhesiri S, Brik A, Shabat D: **Synthesis and evaluation of ubiquitin–dioxetane conjugate as a chemiluminescent probe for monitoring deubiquitinase activity**. *Bioconjugate Chem* 2021, **32**:2141–2147.

48. Jones KA, Kentala K, Beck MW, *et al.*: **Development of a split esterase for protein–protein interaction-dependent small-molecule activation**. *ACS Cent Sci* 2019, **5**:1768–1776.

49. Svehlova K, Lukšan O, Jakubec M, Curtis EA: **Supernova: a deoxyribozyme that catalyzes a chemiluminescent reaction**. *Angew Chem Int Ed* 2022, https://doi.org/10.1002/anie.202109347.

50. Yao Z, Brennan CK, Scipioni L, *et al.*: **Multiplexed bioluminescence microscopy via phasor analysis**. *bioRxiv* 2021.2021.2006.2018.448905.

51. Ogoh K, Akiyoshi R, May-Maw-Thet, *et al.*: **Bioluminescence microscopy using a short focal-length imaging lens**. *J Microsc* 2014, **253**:191–197.

52. Kim TJ, Tuerkcan S, Ceballos A, Pratx G: **Modular platform for low-light microscopy**. *Biomed Opt Express* 2015, **6**:4585–4598.

53. Kim TJ, Türkcan S, Pratx G: **Modular low-light microscope for imaging cellular bioluminescence and radioluminescence**. *Nat Protoc* 2017, **12**:1055–1076.